

RESEARCH ARTICLE

Phenomenological Interpretations of Some Somatic Temporal and Spatial Patterns of Biophoton Emission in Humans

DAQING PIAO

daqing.piao@okstate.edu

School of Electrical and Computer Engineering; and Center for Veterinary Health Sciences, Oklahoma State University, Stillwater, Oklahoma, USA

Submitted October 10, 2019; Accepted January 27, 2021; Published June 15, 2021

<https://doi.org/10.31275/20211685>

Creative Commons License CC-BY-NC

Abstract—Biophoton emission in humans remains intriguing in terms of the temporal and spatial patterns that indicate influences from environmental, physiological, and pathological factors, and even intentional faculty. We propose an analytical hypothesis for interpreting a few patterns of somatic steady-state biophoton emission from humans, including dependency on age, diurnal variation, and geometric asymmetry associated with serious asymmetrical pathological conditions. The analyses are based on associating a hypothetical collective state of autonomic neuro-energy, presented in a form of “vivodensity,” with photo-genesis of biophoton emission. The vivodensity refers to the maximal coherence among the energy “modes” of neuronal control that one can engage in at a given time of life. This vivodensity is treated to modulate metabolic activities responsible for photo-genesis manifested as biophoton emission. The hypothesis projects a decrease of the vivodensity in humans during growth beyond puberty. The hypothesis also proposes a modification of the vivodensity by systemic or homeostatic physiology. The hypothesis further postulates that the deviation of the physiology-modified vivodensity from the prepuberty level is a deterioration due to organ-specific pathological conditions. A temporal differential change of vivodensity is hypothesized to proportionally modulate oxidative stress that functions as the physical source of biophoton emission. The resulting steady-state diffusion of the photon emitted from a photo-genic source in human geometry simplified as a large homogeneous spherical domain is mod-

eled by photon diffusion principles incorporating an extrapolated zero-boundary condition. Age and systemic physiology combined determine the intensity of the center-located physiological steady-state photo-genic source. An acquired pathology sets both the intensity and the off-center position of the pathological steady-state photo-genic source. When the age-commemorated, physiology-commanded, and pathology-controlled modifications of the steady-state photo-genic sources are implemented in the photon diffusion model, the photon fluence rate at the surface of the human-representing spherical domain reveals the patterns of age, the temporal variation corresponding to systemic physiology, and the geometric asymmetry associated with significant asymmetric pathological conditions as reported during spontaneous biophoton emission. The approach, which has the convenience of quantitative estimation of biophoton emission patterns with the potential to incorporate autonomic neuromodulation, may offer novel insights into biophoton phenomena wherein human faculty constitutes an experimental condition.

Keywords: biophoton emission; age; temporal variation; asymmetry; analytical model; photon diffusion; steady state

INTRODUCTION

Biophoton emission (Cifra & Pospisil, 2014) has been investigated over several decades under a variety of terms including the following: weak luminescence (Quickenden & Que Hee, 1974), low-level chemiluminescence (Cadenas et al., 1980), spontaneous chemi-luminescence (Boveris et al., 1984), biophoton(s) emission (Cohen & Popp, 1997; Devaraj et al., 1997), ultra-weak bioluminescence (Wang & Yu, 2009), auto-luminescence (Havaux et al., 2006), spontaneous ultra-weak light emission (Moraes et al., 2012), etc. The spectrum of biophoton emission is interestingly very broad, spanning the visible band, and extending in both directions to ultraviolet and near-infrared bands (Boveris et al., 1980; Cadenas et al., 1980; Cadenas, 1984; Gallas & Eisner, 1987; Devaraj et al., 1997; Kayatz et al., 2001; Fedorova et al., 2007; Kalaji et al., 2012; Kobayashi et al., 2016; Wang et al., 2016; Zhao et al., 2017).

Several theories have been postulated about the origin of biophotons. Perhaps the most widely regarded is that the broadband biophoton radiation can be attributed to the transition of excited biological molecules, primarily reactive oxygen species (ROS)

(Kobayashi et al., 2014). ROS are generated at a fixed rate by oxidation reduction reactions during cellular respiration, but they are toxic to living cells. When in homeostasis, the cellular organism employs a variety of scavenging mechanisms to maintain a relatively consistent concentration of ROS at very low levels (Kobayashi et al., 2014). The luminescence intensity of the baseline spontaneous biophoton emission of a living organism including humans is thus extremely low, on the order of hundreds of photons per square centimeter per second (Cohen & Popp, 1997; Zhang et al., 1997) when measured on the surface, whereas the intra-organism intensity has been speculated to possibly be substantially higher (Bokkon et al., 2010). For a photon at the visible wavelength of 500 nm, a photon count rate of 100 photons per second per square centimeter corresponds to an irradiance of $3.98 \times 10^{-17} \text{ W} \cdot \text{cm}^{-2}$ or $\sim 0.04 \text{ fW} \cdot \text{cm}^{-2}$. This irradiance is comparable to the photon fluence rate measured at 10 cm from a localized source of $1 \mu\text{W} \cdot \text{cm}^{-3}$ in an unbounded homogeneous tissue medium having an absorption coefficient of 0.106 cm^{-1} and a reduced scattering coefficient of 10 cm^{-1} that are representative of soft tissue. The extremely small intensity makes spontaneous biophoton emission challenging to detect without highly sensitive photon-detecting devices carefully configured in a completely darkened environment.

In spite of the challenges in biophoton detection due to the ultraweak intensity, significant efforts and progress have been made in mapping biophotons from various regions of the human body (Ives et al., 2014). Many of these results indicated the potential of mapping biophotons for assessing holistic health, based upon some systemic patterns that biophotons from humans manifest. The variations of spontaneous biophoton emission intensity from humans in association with normal physiological phases or environmental influences have been reported on different temporal scales. Diurnal rhythms of spontaneous biophoton emission of humans have been linked to the systemic changes in energy metabolism inherent to a circadian cycle (Kobayashi et al., 2009). Frequency analysis of the spontaneous biophoton emission intensity revealed temporal characteristics with slow-periodicity components longer than 24 hours ranging from 7 days to 270 days (Cohen & Popp, 1997; Cohen & Popp, 2003). Seasonal variation of spontaneous biophoton emission intensity (Zheng et al.,

1983; Cohen & Popp, 2003; Jung et al., 2005) revealed as high as 4-fold changes over year-long measurements, with the lowest intensity in the autumn and the highest intensity appearing 6 months from autumn. Spontaneous biophoton emission has also manifested gender and age-related variations (Yang et al., 1995; Yang et al., 1996; Sauermann et al., 1999; He et al., 2016; Zhao et al., 2016). Biophoton emission intensity was observed to be higher among males than among females, and higher in adults than in children. The aged male adult had ~40% higher biophoton emission intensity than the aged female adult (He et al., 2016). The biophoton emissions of both males and females starts to increase by the age of 11–14 and stabilizes at about age 50 (He et al., 2016). These findings indicate that measuring biophoton emission can potentially provide insight into the homeostatic state or systemic stage, as well as the harmonic correlation between the human body and the environment that is regarded as fundamental in some alternative medical and healing practices (Sun et al., 2017). Deviations from spontaneous biophoton emission intensity from these healthy temporal rhythms thus may render information on the deviation of the systemic or homeostatic physiological states from normal levels.

The temporal variations of the human spontaneous biophoton emission intensity of normal physiological states also implies that a human state departing significantly from healthy conditions due to acquired pathology may manifest in variations of biophoton emission intensity that could be much stronger and potentially much more varied than those from a systemic cause. An acquired pathology that is not systemic but is organ- or tissue-confined could also cause the spontaneous biophoton emission pattern to be altered from a healthy balanced or symmetric configuration. An alteration of the biophoton emission by acquired organ- or site-specific pathology is likely to break the symmetry of the spontaneous biophoton emission expected for a balanced faculty. For example, a multiple sclerosis case was found to give ~200 biophoton counts/second in the right hand and ~300 biophoton counts/second in the left hand (Cohen & Popp, 1997). For hemiparesis patients, the hand with a hemiparesis aspect emitted fewer biophotons in comparison with the contra-lateral normal hand (Jung et al., 2003), and acupuncture treatment dramatically reduced the left–right asymmetry of biophoton emissions. The left–right asymmetry of

spontaneous biophoton emission in a mouse model of human breast cancer (Zhao et al., 2017) became more pronounced as the tumor load in the right axillary increased versus the contra-lateral normal side. These reports appear to suggest that the left–right asymmetry of spontaneous biophoton emission correlates with left–right pathological differences.

Additionally, a particularly intriguing presentation of biophotons in association with humans cannot be missed: The biophoton intensity seems to be modulated by intention or human interaction during healing or other various kinds of bioenergy practices (Nakamura et al., 2000; Haraguchi et al., 2001; Joines et al., 2012; Rubik & Jabs, 2017). Links have also been suggested between biophotons and observations that are difficult to measure and quantify, including consciousness (Rahnama et al., 2011), mind–matter manipulation (Caswell et al., 2014; Pederzoli et al., 2017), and paranormal phenomena at the moment of death (Persinger & St-Pierre, 2011; Reddy, 2016). One could argue that an experimental control that appears common to all these phenomena is the involvement of human factors, which at the physical level will reside in the engagement of neuronal activities, no matter whether autonomic or intentional. The variation in surface biophoton emission has been known to correlate with changes in metabolism. When living organisms become stressed (Slawinski et al., 1992; Musumeci et al., 1997), the ROS varies to subsequently change biophoton emission (Tsuchida et al., 2019). Induced changes in photon emissions offer physiologically relevant explanations for some human experiences that are often inexplicable even though not uncommon, including the entopic phenomena of phosphene and negative afterimage (Bokkon et al., 2011; Wang et al., 2011; Salari et al., 2017). Studies have also suggested that ROS may be signaling agents, rather than simply potential toxic agents (Rice et al., 2002). Whether ROS are signaling or toxic agents, the variation of the rate of the production of ROS in humans will be regulated ultimately by autonomic neuromodulation, which will likely differ at different stages of life and also be perturbed or affected by environmental factors and acquired conditions. Variations in biophoton emissions due to variations of ROS then shall be expected to follow the temporal paces as well as spatial patterns of the neuromodulating perturbation causing autonomic adaptation of ROS production, with a potential delay in the phase of change as is conceptualized in Figure 1.

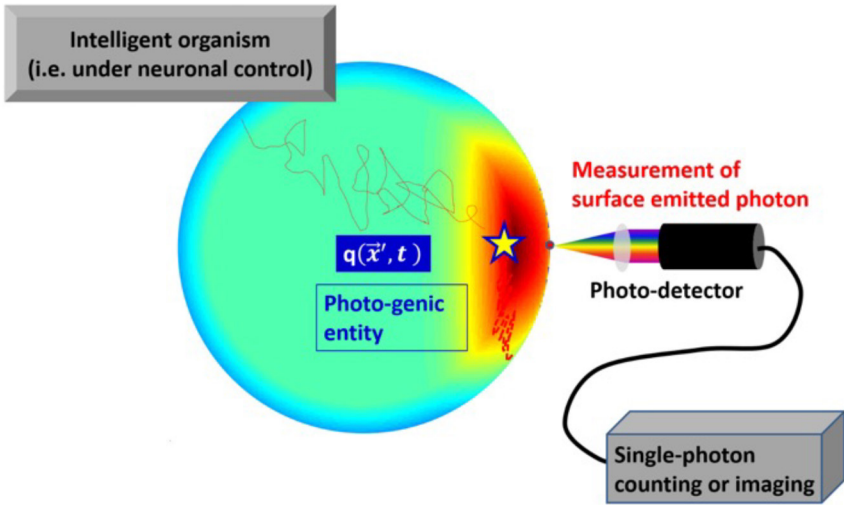


Figure 1. Conceptual illustration of the surface measurement of a biophoton from a human, representing a large intelligent organism. What is acquired by the photon-counting or imaging devices is the photons emitting from the surface of the organism. The origin of the surface-emitted biophotons may be at any location within human tissue, wherein a localized photo-genic entity engaging ROS may occur.

In this work, we propose an analytical framework of hypotheses with the objective to provide simple interpretations of a few somatic temporal and spatial patterns of spontaneous biophoton emission in humans, including the systemic dependency on age, the diurnal variation, and the geometric asymmetry associated with serious asymmetrical pathological conditions. The analysis speculates that there is a collective state of autonomic neuro-energy expressed in a form of “vivodensity,” which in essence is the maximal coherence among the energy “modes” of neuronal control that an intelligent being represented by humans is able to engage in at any given time of life. This vivodensity could also be considered as being proportional to a chemical potential of the metabolic aspect (Piao, 2020b) which regulates how a systemic perturbation to metabolism is transferred to a local photo-genesis process to cause observable temporal changes in biophoton emission. This vivodensity thus is treated to modulate metabolic activities responsible for photo-genesis pertinent to biophotons. The hypothesis projects a decrease in the vivodensity

in humans during growth beyond puberty, with the rate of decrease dictated by a time constant set by the date of sexual maturity. The hypothesis also proposes a modification of the vivodensity by the phases of systemic or homeostatic physiology. The hypothesis further postulates that the deviation of the physiology-modified vivodensity from the pre-puberty level is deteriorated by acquired organ-specific pathological conditions. The temporal differential change of vivodensity is projected to be photo-genic, by proportionally modulating oxidative stress that functions as the physical source of biophoton emission. The age and systemic physiology combined determines the intensity of the physiological photo-genic source that is simplified as being centrally located within the body for analytical simplicity. An acquired pathology sets both the intensity and generally an off-center position of the pathological photo-genic source. The light emission from a photo-genic source, wherever it is within the tissue, then must diffuse through the human body in the process of propagating to the surface before being detected. The human tissue involved in biophoton propagation is treated as a homogeneous translucent spherical domain for analytical convenience. The diffusive photon propagation in tissue is modeled according to photon diffusion principles that account for scattering and absorption of bulk tissue and incorporates an extrapolated zero-boundary condition. When the age-commemorated, physiology-commanded, and pathology-controlled modifications of the photo-genic sources are implemented in the steady-state photon diffusion model, the steady-state photon-fluence rate at the surface of the human-simplifying spherical domain can reveal the patterns of intensity dependence upon age, variations corresponding to systemic physiology, and geometric asymmetry associated with significant asymmetric pathological conditions as reported in experimental spontaneous biophoton emission studies.

A HYPOTHESIS ON NEURO-MODULATED PHOTO-GENIC SOURCING OF BIOPHOTON EMISSION

The scope of this work is to offer alternative insights on some temporal and spatial patterns of biophoton emission in humans, which indubitably represents the highest level of intelligence among

organisms. We consider intelligence to be uniquely and ubiquitously associated with neuronal activity that ceases when the organism loses metabolic ability to excite or inhibit a neuronal firing. We represent the condition of a neuron with respect to its normal activated state (in either full excitatory or full inhibitory phase [Wilson & Cowan, 1972]) by a phasor term of

$$n_i(\vec{\chi}, t) = A(\vec{\chi}) \cdot \exp[j\phi(t)] \quad (1)$$

where $i = [0, N_{total}]$ of which N_{total} is the total number of originally intact neurons. Denoting $N_{live}(t)$ as the number of viable neurons at a given time, we would have $N_{live}(t) \leq N_{total}$ due to neurodegeneration. Apparently, the proportion of the viable neurons with respect to the total number of originally intact neurons must be bounded in $[0, 1]$. We choose a simple function to represent this dimensionless neuronal viability as the following

$$\eta_{viab}(t) = \frac{N_{live}(t)}{2N_{total} - N_{live}(t)} \quad (2)$$

The condition $\eta_{viab} = 1$ would indicate that all native neurons are intact, and $\eta_{viab} = 0$ would mark the complete death of the entire set of neurons. Note that Eq. (2) is not the exclusive form of η_{viab} in representing the proportion of viable neurons over the course of life. We further introduce a degree of coherence (dimensionless) to mark how well the neuronal activities are coordinated at a given time, as the following:

$$\xi_{cohe}(\vec{\chi}, t) = \prod_{n_1 \neq n_2}^{\vec{\chi}} \frac{\langle n_1^*(\vec{\chi} - \vec{x}_1, t) \cdot n_2(\vec{\chi} - \vec{x}_2, t + \tau) \rangle}{\sqrt{[n_1^*(\vec{x}_1, t) \cdot n_1(\vec{x}_1, t)] \cdot [n_2^*(\vec{x}_2, t) \cdot n_2(\vec{x}_2, t)]}} \quad (3)$$

where the $\langle \dots \rangle$ of the numerator indicates temporal averaging. The $\vec{\chi}$ in the argument does not change the value of the time-averaging but will remain for a future need to address neuronal activities for regulating a specific metabolism. This $\xi_{cohe}(\vec{\chi}, t)$ also has a value of $[0, 1]$. The condition of $\xi_{cohe} = 0$ indicates spontaneous neuronal activities that are completely random, while $\xi_{cohe} = 1$ marks the condition impossible

to reach with the activation of the entire set of neurons being exactly in-phase. We then hypothesize that the live state of a human can be treated as being associated with a collective state of autonomic neuro-control in a scale of “vivodensity,” which has a spatially and temporally resolved scalar value of $\mathbb{E}_{vivo}(\vec{\chi}, t)$ (unit: $J \cdot cm^{-3}$) at a spatial position $\vec{\chi}$ and a time t . The scalar “vivodensity” $\mathbb{E}_{vivo}(\vec{\chi}, t)$ takes the following form:

$$\mathbb{E}_{vivo}(\vec{\chi}, t) = \eta_{viab}(t) \times \xi_{cohe}(\vec{\chi}, t) \times \mathbb{P}_{mode}(\vec{\chi}, t) \quad (4)$$

which includes a total mode-density $\mathbb{P}_{mode}(\vec{\chi}, t)$ (unit: $J \cdot cm^{-3}$)

represented by the following

$$\mathbb{P}_{mode}(\vec{\chi}, t) = \int \mathcal{P}(\vec{\chi}, t, \nu) d\nu \quad (5)$$

where $\mathcal{P}(\vec{\chi}, t, \nu)$ is a mode-distribution function at a frequency ν of neuron firing. The vivodensity $\mathbb{E}_{vivo}(\vec{\chi}, t)$ essentially defines the maximal coherence among the energy “modes” of neuronal control that an organism of intelligence is entitled to engage in. It can be expected that the ability of autonomic neuro-control degrades as an intelligent being ages, and the value represented by Eq. (4) shall decrease over age and recede to zero at the cease of the life. According to the declining survival rate of the human being as a function of age that becomes pronounced at older ages (Sarna et al., 1993), we regard the natural course from birth to death of human life to experience three systemic changes that may occur synchronously: (1) the initial healthy increase and later matured stabilization of the body volume-contents, (2) the temporal variation of the biological phases by endocrine and exocrine controls, and (3) the deterioration of the body functions due to acquired pathological conditions. We will then represent the course of change of $\mathbb{E}_{vivo}(\vec{\chi}, t)$ as

$$\mathbb{E}_{vivo}(\vec{\chi}, t) = \mathbb{Z}_{prim}(\vec{\chi}, t) \mathbb{H}_{syst}(\vec{\chi}, t) [1 - \mathbb{U}_{path}(\vec{\chi}, t) \cdot \mathbb{N}_{auto}(\vec{\chi}, t)], \quad (6)$$

where $\mathbb{Z}_{prim}(\vec{\chi}, t)$ (unit: $J \cdot cm^{-3}$) denotes the “primo” state of

“vivodensity” inherited from birth, $\mathbb{H}_{\text{sys}}(\vec{\chi}, t)$ (unit: dimensionless) represents the phase of the systemic or homeostatic physiology that is endogenous to a healthy subject, $\mathbb{U}_{\text{path}}(\vec{\chi}, t)$ (unit: dimensionless) accounts for the effect of an acquired pathology that is exogenous to an otherwise healthy subject, and $\mathbb{N}_{\text{auto}}(\vec{\chi}, t)$ (unit: dimensionless) marks the terminal autonomic control of the site pertinent to the acquired pathology. The basic declining behaviors of $\mathbb{E}_{\text{vivo}}(\vec{\chi}, t)$ from the “primo” level at birth due to aging and systemic physiology and acquired pathology are conceptualized in Figure 2. Panel (A) marks the initial level of “vivodensity” set at birth. Panel (B) specifies the decrease of “vivodensity” as a result of growth and aging. Panel (C) represents the deviation of “vivodensity” from the age-related level due to modulation by systemic physiology. Panel (D) manifests the degradation of “vivodensity” from the healthy level for a particular age caused by acquired pathology.

Additionally, there are the needs of several absolute time-points or characteristic ages of the course of natural human life that are symbolized as the following: t_{birth} is the time of birth, t_{death} is the time of death, t_{puber} is the time of puberty, so $\tau_{\text{life}} = t_{\text{death}} - t_{\text{birth}}$ is the life span and $\tau_{\text{puber}} = t_{\text{puber}} - t_{\text{birth}}$ is the age when puberty starts. At one’s birth, the following initial conditions of the entities shall be relevant: $\mathbb{Z}_{\text{prim}}(\vec{\chi}, t_{\text{birth}}) = \mathbb{Z}_0$, $\mathbb{H}_{\text{sys}}(\vec{\chi}, t_{\text{birth}}) = 1$, and $\mathbb{U}_{\text{path}}(\vec{\chi}, t_{\text{birth}}) = 0$ and $\mathbb{N}_{\text{auto}}(\vec{\chi}, t_{\text{birth}}) = 1$. The values of these parameters over the lifespan of the person for $t \in (t_{\text{birth}}, t_{\text{death}}]$ is further constrained respectively as the following:

$$\begin{aligned} \mathbb{Z}_{\text{prim}}(\vec{\chi}, t) \in [0, \mathbb{Z}_0], \mathbb{H}_{\text{sys}}(\vec{\chi}, t) \in (0, 1], \mathbb{U}_{\text{path}}(\vec{\chi}, t) \in [0, 1] \\ \text{and } \mathbb{N}_{\text{auto}}(\vec{\chi}, t) \in [0, 1]. \end{aligned}$$

A pathological condition that is terminal or lethal is represented by $\mathbb{U}_{\text{path}}(\vec{\chi}, t) = 1$. A normal autonomic control of a site in a pathological condition is marked by $\mathbb{N}_{\text{auto}}(\vec{\chi}, t) = 1$. The complete loss of the autonomic control at the site of a pathological condition is demarcated by $\mathbb{N}_{\text{auto}}(\vec{\chi}, t) = 0$.

For the normal course of a human life, it is reasonable to assume that a life-shortening pathology is acquired after puberty, and the “primo” state of the vivodensity $\mathbb{Z}_{\text{prim}}(\vec{\chi}, t)$ from birth to puberty would be sustained at the initial level of \mathbb{Z}_0 set at birth with the

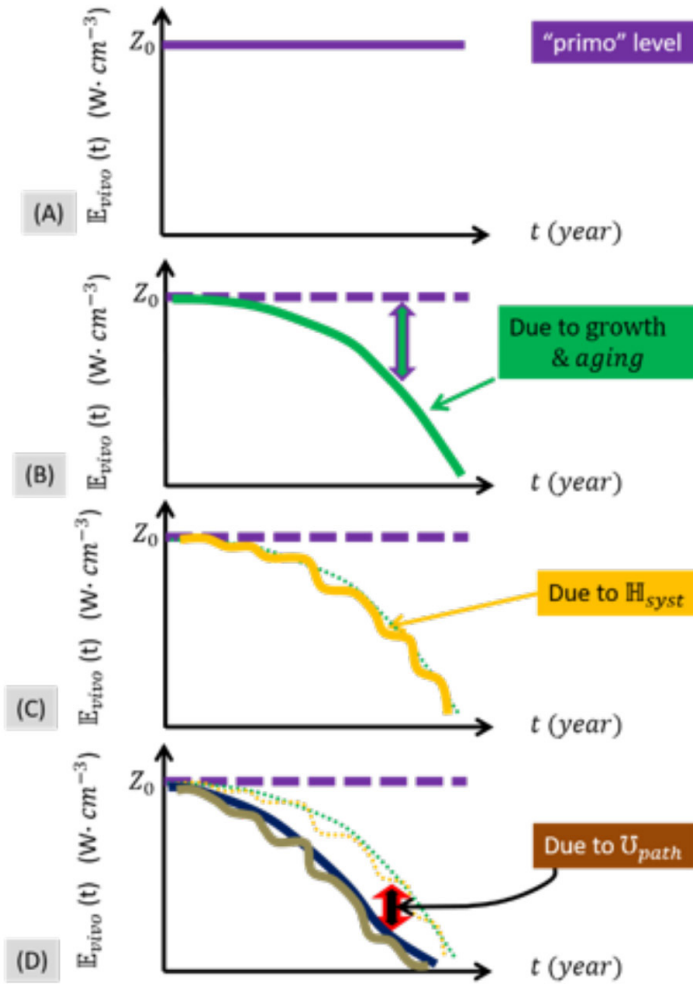


Figure 2. (A) The “vivodensity” bestowed on a person at birth. (B) The decrease of the vivodensity of a healthy person due to aging. (C) The modulation of the vivodensity of a healthy person by systemic physiology. (D) The degradation of the vivodensity of a person from the healthy level by acquired pathology.

only modification incurred due to systemic or homeostatic physiology $H_{syst}(\vec{\chi}, t)$. This results in a level-set representation of the vivodensity as the following, with the use of the Heaviside or unit step function $u(t)$:

$$E_{vivo}(\vec{\chi}, t) = Z_0 [u(t - t_{birth}) - u(t - t_{puber})] H_{syst}(\vec{\chi}, t) + Z_{adol}(\vec{\chi}, t) [u(t - t_{puber}) - u(t - t_{death})] H_{syst}(\vec{\chi}, t) [1 - U_{path}(\vec{\chi}, t) N_{auto}(\vec{\chi}, t)] \tag{7}$$

where $Z_{adol}(\vec{\chi}, t)$ specifies the “primo” state of the vivodensity counted from τ_{puber} as the person enters “adolescence,” which decreases from the “primo” level as the following:

$$Z_{adol}(\vec{\chi}, t) = Z_0\{1 - \boxtimes(\vec{\chi}, t)\} \tag{8}$$

where $\boxtimes(\vec{\chi}, t) \leq 1$ is a non-negative value corresponding to the amount of degradation of $Z_{adol}(\vec{\chi}, t)$ when compared to Z_0 . We define the temporal differential deviation of vivodensity from the systemic physiology modified birth state of Z_0 over the lifetime as the following:

$$\frac{\partial}{\partial t} [\Delta Z_{vivo}(\vec{\chi}, t)] = \frac{\partial}{\partial t} [Z_0 \mathbb{H}_{syst}(\vec{\chi}, t) - \mathbb{E}_{vivo}(\vec{\chi}, t)] \tag{9}$$

By using Eq. (7), it is straightforward to obtain the following:

$$\begin{aligned} \frac{\partial}{\partial t} [\Delta Z_{vivo}(\vec{\chi}, t)] &= \left\langle \frac{\partial}{\partial t} \{ [Z_0 - Z_{adol}(\vec{\chi}, t)] \mathbb{H}_{syst}(\vec{\chi}, t) \} [u(t - t_{puber}) - u(t - t_{death})] \right. \\ &+ \left. \left\langle \frac{\partial}{\partial t} \{ Z_{adol}(\vec{\chi}, t) \mathbb{H}_{syst}(\vec{\chi}, t) \mathbb{U}_{path}(\vec{\chi}, t) \mathbb{N}_{auto}(\vec{\chi}, t) \} [u(t - t_{puber}) - u(t - t_{death})] \right. \right. \\ &\tag{10} \end{aligned}$$

Two entities of differential properties are introduced as shown, respectively, in the following:

$$\frac{\partial}{\partial t} [\Delta Z_{adol}(\vec{\chi}, t)] = Z_0 \frac{\partial}{\partial t} [\boxtimes(\vec{\chi}, t) \cdot \mathbb{H}_{syst}(\vec{\chi}, t)] \tag{11}$$

$$\frac{\partial}{\partial t} [\Delta \mathbb{U}_{path}(\vec{\chi}, t)] = -Z_0 \frac{\partial}{\partial t} [\boxtimes(\vec{\chi}, t) \cdot \mathbb{H}_{syst}(\vec{\chi}, t) \mathbb{U}_{path}(\vec{\chi}, t) \mathbb{N}_{auto}(\vec{\chi}, t)] \tag{12}$$

Equation (9) then becomes

$$\begin{aligned} \frac{\partial}{\partial t} [\Delta Z_{vivo}(\vec{\chi}, t)] &= \left\{ \frac{\partial}{\partial t} [\Delta Z_{adol}(\vec{\chi}, t)] \right. \\ &+ \left. \frac{\partial}{\partial t} [\Delta \mathbb{U}_{path}(\vec{\chi}, t)] \right\} [u(t - t_{puber}) - u(t - t_{death})] \tag{13} \end{aligned}$$

where the first “differential” component associated with $Z_{adol}(\vec{\chi}, t)$

as specified by Eq. (11) denotes the temporal deviation of the “vivodensity” from the “primo” state as a result of normal biological development, and the second “differential” component associated with ΔU_{path} as specified by Eq. (12) represents the further temporal deviation of the “vivodensity” from the normal level for a particular age due to acquired pathology.

Eq. (13) by referring to Eqs. (11) and (12) will infer the age-dependency of the temporal differentiation of \mathbb{Z}_{vivo} by setting $\mathbb{H}_{syst}(\vec{\chi}, t) = 1$ and $\mathbb{U}_{path}(\vec{\chi}, t) = 0$, the effect of systemic physiology over a time period by setting $\mathbb{U}_{path}(\vec{\chi}, t) = 0$, and the outcome of acquired pathology at a given time point by setting $\mathbb{H}_{syst}(\vec{\chi}, t) = 1$.

We further hypothesize the vivodensity to be proportional to a chemical potential of the metabolic aspect (Piao, 2020b) which may regulate how a systemic perturbation to metabolism is transferred to a local photo-genesis process to cause observable temporal changes in biophoton emission, through the oxidative bio-chemical pathways that produce free radicals with ROS (Slawinski et al., 1992; Burgos et al., 2016). And this chain reaction can be treated as the changing rate of “vivodensity” that modulates oxidative stress. Integrating the spatially resolved temporal differentiation of the “vivodensity” changes represented by Eqs. (11) and (12) over the body-scaled volume gives rise to two spectrally and temporally resolved photo-genic intensity terms to be assigned as the sources of photo-genesis:

$$\mathbb{S}_{syst}(\lambda, t) = \varrho_{syst}(\lambda, t) \iiint \frac{\partial}{\partial t} [\Delta \mathbb{Z}_{adol}(\vec{\chi}, t)] d\vec{\chi}^3 \quad (14)$$

$$\mathbb{S}_{path}(\lambda, t) = \delta_{path}(\lambda, t) \iiint \frac{\partial}{\partial t} [\Delta \mathbb{U}_{path}(\vec{\chi}, t)] d\vec{\chi}^3 \quad (15)$$

where $\varrho_{syst}(\lambda, t)$ (unit: cm^{-3}) is the spectrally and temporally resolved physiological-photo-genic volumetric transfer-factor, and $\delta_{path}(\lambda, t)$ (unit: cm^{-3}) is the spectrally and temporally resolved pathological-photo-genic volumetric transfer-factor. For simplicity, we treat the human body as a volume of spherical domain of radius R_0 as shown in Figure 3. The physiological photo-genic source \mathbb{S}_{syst} (unit: $\text{W} \cdot \text{cm}^{-3}$) is set at the center of the spherical domain, whereas the pathological photo-genic source \mathbb{S}_{path} (unit: $\text{W} \cdot \text{cm}^{-3}$) that may be

weighted for a single, serious, organ-specific pathology could be positioned at any distance R_{path} to the center. The spherical coordinates of the pathological photo-genic source S_{path} are set as $(R_{path}, \theta', \phi')$, or for convenience of visualization at the 3 o'clock position with respect to the center of the spherical body. The spectral and temporal dependences of the photo-genic sources S_{syst} and S_{path} are not considered in this work, i.e.,

$$q_{syst}(\lambda, t) = q_{syst} = \text{constant}, \quad \delta_{path}(\lambda, t) = \delta_{path} = \text{constant},$$

thus S_{syst} and S_{path} are steady-state sources that will facilitate analysis of the simplest steady-state photon propagation in body volume.

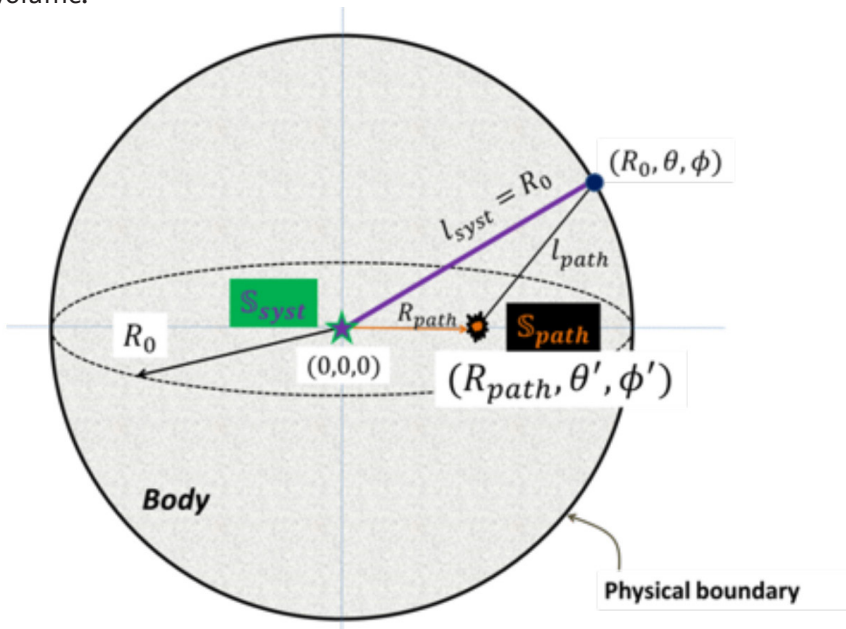


Figure 3. The human body is simplified as a geometric sphere with a radius R_0 . The physiological photo-genic source S_{syst} is set at the center of the spherical domain, or with the spherical coordinates of $(0,0,0)$. The pathological photo-genic source S_{path} is at (R_0, θ, ϕ) which is positioned at the 3 o'clock position with respect to the spherical center, at $(R_{path}, 0, 0)$. The distance of any position on or off the spherical surface to the pathological source S_{path} is denoted as l_{path} .

NUMERICAL EVALUATION OF STEADY-STATE SURFACE PATTERNS OF BIOPHOTON EMISSION

We show in the Appendix how the steady-state diffusion of light with spectral relevancy to spontaneous biophoton emission (i.e., in the VIS/NIR band of the biological window for which the photon diffusion analysis is conventional) is treated with the necessary approximation to facilitate numerical evaluation of the problem in a spherical human-size tissue geometry with the pertinent boundary condition. In this section, we use the photo-genic terms of Eqs. (14) and (15) to illustrate the general bulk surface pattern, which manifests an aura-like hue, of steady-state biophoton emission.

Eq. (A13) (Appendix) can be implemented numerically to assess the patterns of steady-state photon-fluence rate presenting at or beyond the air-interfacing boundary of the human-representing spherical homogeneous tissue domain, in association with the physiological photo-genic source $\mathbb{S}_{\text{sys}t}$ alone or with the addition of the pathological photo-genic source \mathbb{S}_{path} . The distribution of the steady-state photon-fluence rate across the surface of the human-representing spherical domain and expanding to the extrapolated zero-boundary is exemplified in Figure 4. The tissue medium used for all numerical evaluations in this section is specified with the following dimensional and optical properties: a radius of $R_0 = 10 \text{ cm}$, an absorption coefficient of $\mu_a = 0.1 \text{ cm}^{-1}$, a reduced scattering coefficient of $\mu'_s = 10 \text{ cm}^{-1}$, and a refractive index of $n = 1.4$. The tissue optical properties result in a distance of $R_b = 0.11 \text{ cm}$ of the extrapolated zero-boundary from the tissue boundary, which is only 1.1% of the radius of the spherical domain. When the tissue medium represented by the spherical domain contains only the centered physiological photo-genic source $\mathbb{S}_{\text{sys}t}$, the photon-fluence rate on the entire spherical boundary has to be circumferentially uniform, and the photon-fluence rate will decrease from the tissue boundary to become zero at the extrapolated zero-boundary. The degradation of the steady-state photon-fluence rate from the tissue boundary to the extrapolated zero-boundary over an entire azimuthal or elevational circle will appear as a thin circular strip (i.e., aura-like hue) of 0.11 cm thick around the spherical tissue domain. To better visualize this thin circular strip of the

steady-state photon-fluence rate around the spherical tissue domain in Figure 4, the evaluation of Eq. (A13) over the space beyond the tissue boundary is conducted over a radial distance of 10 times of R_b , i.e., a 1.1-cm distance from the tissue boundary as the strip of lower color value outside the dashed circle demarcating the spherical tissue boundary. In obtaining Figure 4, the following additional parameters are necessary: $S_{syst} = 0.01\mu W \cdot cm^{-3}$ and $S_{path} = 0$. The circumferentially uniform photon-fluence rate across the spherical tissue domain represents the 2-dimensional projection of the photon-fluence rate measured on the surface of the spherical tissue domain, as is the case for measurement/imaging using a planar, pixelated photon-detection device. The steady-state photon-fluence rate projected on the surface of a spherical tissue domain of the associated optical properties with a 10-cm radius and an extremely weak source of $0.01\mu W \cdot cm^{-3}$ at the center is at the level of $1 \times 10^{-17} W \cdot cm^{-2}$ (corresponding to 25

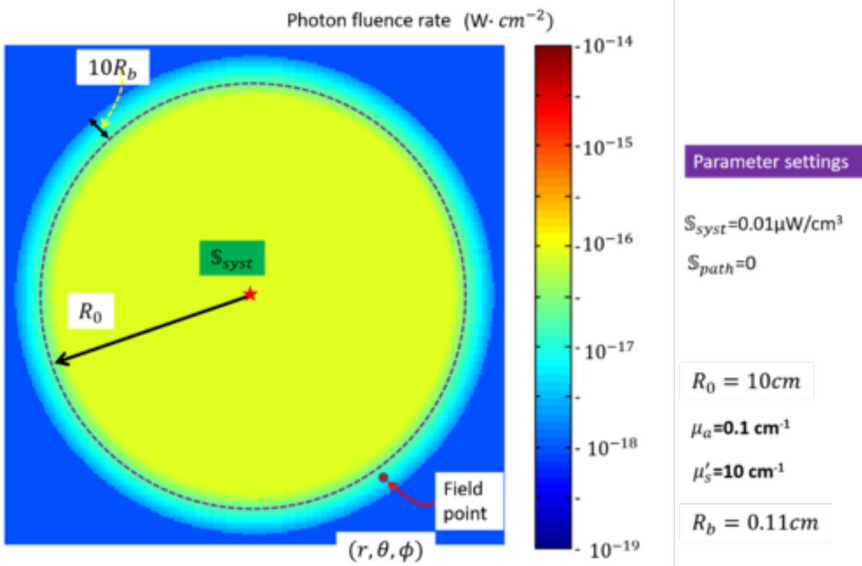


Figure 4. Example of the distribution of the photon-fluence rate across the surface of the human-representing spherical domain and expanding to the extrapolated boundary. The degradation of the photon-fluence rate from the tissue boundary to the extrapolated boundary over an entire azimuthal or elevational circle is illustrated as a thin circular strip around the spherical tissue domain.

counts of 500 nm photons per second per cm^2), and drops to zero at the extrapolated zero-boundary that in actual scale is just about 0.11 cm or 1.1 mm away from the tissue boundary of the specified optical properties. A smaller difference of the refractive index between tissue and air could push the extrapolated zero-boundary away from the tissue to make the hue-like margin broader.

ASSIMILATION OF SOMATIC TEMPORAL AND SPATIAL PATTERNS OF BIOPHOTON EMISSION

In the following sections, we demonstrate how the temporal and spatial patterns of biophoton emission measured on the surface of the spherical domain can be modulated by modulating the photo-genesis to reveal some global or somatic patterns that have been shown to be associated with the activities of intelligent beings including human and rodent models of human disease.

The numerical implementations of Eq. (A13) are configured in three different cases of the photo-genic sources that all change at rates that are extremely slow compared with the time of photon propagation in tissue. This will result in the temporal pace of the surface photon emission to be dictated by the temporal pattern of photo-genesis that may be further modified by the spatial configuration of photo-genesis with respect to the surface measurement (Piao, 2020a). The following analyses will reveal, respectively, the most apparent superficial temporal and spatial patterns of age-dependency, physiological variation, and pathological asymmetry of the steady-state photon-fluence rate at the surface of the spherical domain. It is noted that the macroscopic temporal variation is assessed via relative changes of the steady-state photon-fluence rate evaluated at the same spatial location over a macroscopic timescale that is many orders greater than the time of light propagation in the tissue domain. Therefore, when the steady-state photon-fluence rate is to be evaluated at one position to assess the temporal changes at any macroscopic duration, the position of the field point is set at the spherical tissue boundary and at the 3 o'clock position, and the resulting steady-state photon-fluence rate is normalized by comparing with data from the literature of spontaneous steady-state biophoton emission that are reproduced with the copyrighters' permissions.

Presentation of Age Dependency

In order to simulate age dependency, it is necessary to specify the timescale characteristics of physiological photo-genesis. We define τ_{fossi} as the age of a person's first opposite-sex sexual intercourse (FOSSI). A person who commits heterosexual activities at least once in their life will have $t_{birth} < t_{puber} < (t_{birth} + \tau_{fossi}) < t_{death}$. A person who remains a virgin will have $\tau_{fossi} = (t_{death} - t_{birth}) = \tau_{life}$. We define the systemic photo-genesis of biophoton emission as a result of aging to take the following form

$$S_{syst}(\lambda, t) = \left[1 - \exp\left(-\frac{t}{\tau_{age}}\right) \right]^a \quad (16)$$

where the time constant τ_{age} takes a slowly reducing form represented by the following

$$\tau_{age} = (\tau_{life} - \tau_{fossi}) \exp\left[-\frac{(t - t_{puber}) * H(t - t_{puber})}{\tau_{fossi}}\right] + \tau_{fossi} \quad (17)$$

where a is a positive number or an aging factor. The age dependency and gender difference of the photon-fluence rate at the boundary of the spherical tissue domain is simulated by removing S_{path} and setting the following parameters: the puberty age t_{puber} of males is 13, the puberty age t_{puber} of females is 11, the FOSSI age τ_{fossi} of both males and females is age 20, the aging factor is specified as $a = 2$, and a lifespan is 75 years. The male tissue density is assumed to be greater than the female at the same age, leading to stronger intensity of the physiological photo-genic source S_{syst} for males at otherwise identical settings of the parameters. Alternatively, stronger adipose fat content in females could cause a higher scattering attenuation of the photon propagation to result in less photon emission at the surface of the body under the same physical dimensions and photo-genic conditions. A literature report showing the dependency of spontaneous biophoton counts on age and the difference in biophoton counts between males and females is reproduced with permission from the publisher (He et al., 2016) as shown in Figure 5A. In panel (A) there is a smaller downward-pointing arrow pointing to an age group of 11 to 14 years for both males and females, at which the biophoton count starts

to increase noticeably. That age range is projected to indicate puberty. In panel (A) there is a larger upward-pointing arrow pointing to an age group of 41 to 50 years for the female group that may be interpreted as menopause onset. That menopause-inferring change is not included in the numerical model analysis per se. The numerical results as specified heretofore are plotted in Figure 5(B) with the assumption that the photon-fluence rate has a baseline count at the same levels as in the literature report.

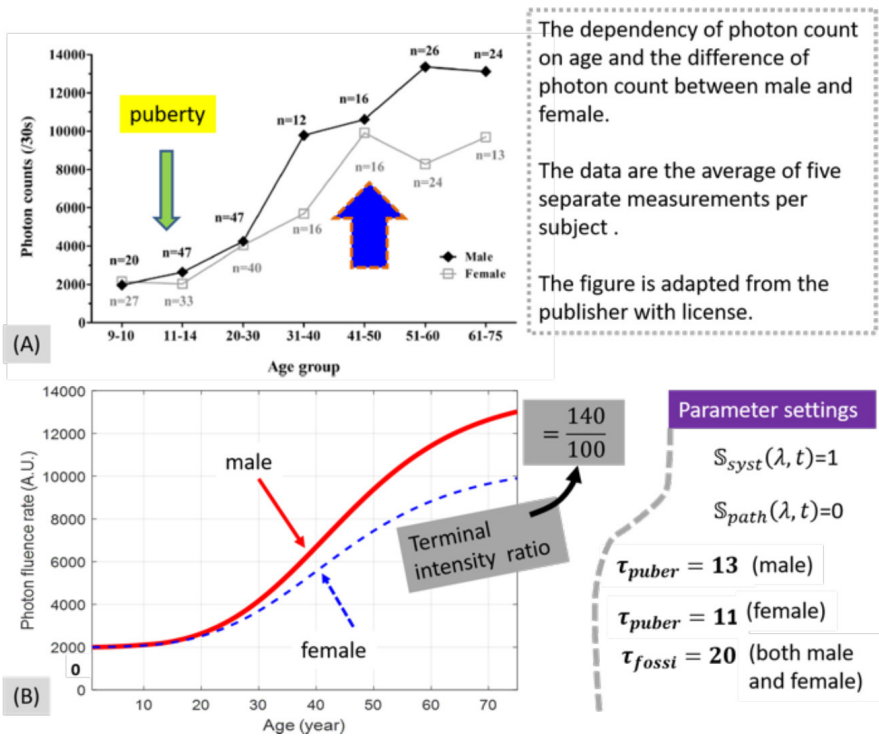


Figure 5. (A) The age dependency and gender difference in biophoton emission, demonstrated in a literature study (He et al., 2016), and (B) the simulated photon-fluence rate at the boundary of the spherical tissue. In panel (A), the small arrow (pointing downward) pointing toward age group 11–14 for both males and females, is the point at which the spontaneous biophoton count started to increase noticeably. That age group is projected to indicate puberty. In (A), the larger upward-pointing arrow points to the female age group 41–50 and may be interpreted as indicating menopause onset.

Presentation of Diurnal Variation

The variation of the photon fluence rate revealed at the boundary of the spherical tissue domain as a function of short-term homeostatic changes over a duration of 24 hours is simulated by removing S_{path} and setting S_{syst} and thus $S_{syst}(\lambda, t)$ to change periodically. A known diurnal variation of the spontaneous biophoton count is adopted from an open access publication (Cifra et al., 2007) as shown in Figure 6(A). The spontaneous biophoton emission intensity revealed a trough in the later afternoon and a peak in early

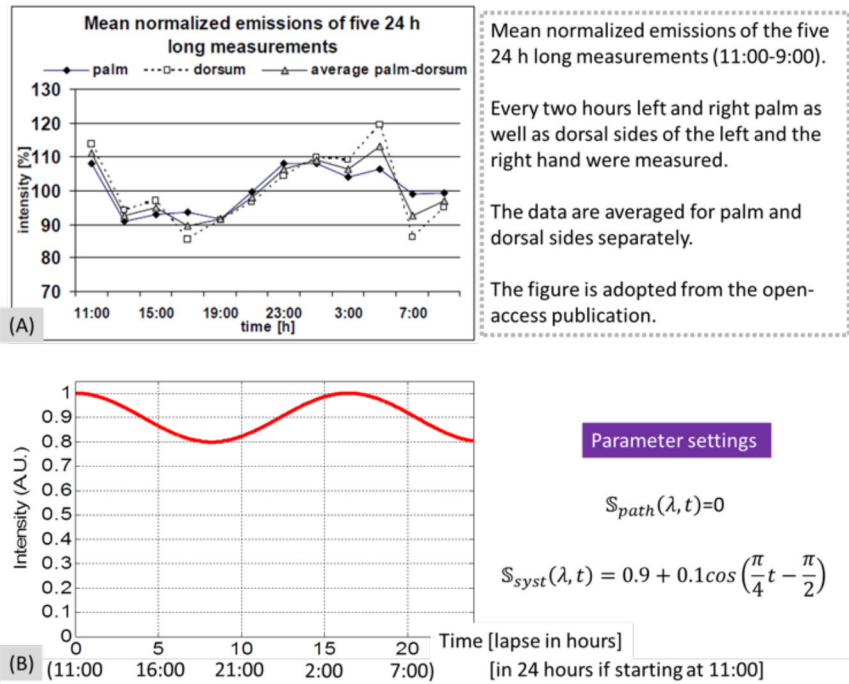


Figure 6. (A) The diurnal variation of biophoton counts adopted from Cifra et al. (2007). The biophoton emission intensity revealed a trough later in the afternoon and a peak in the early morning. That diurnal variation over a range of approximately 90–110% of the mid-line level can be directly associated with the circadian cycle. The variation of the photon-fluence rate revealed at the boundary of the spherical tissue domain as a function of short-term homeostatic changes is simulated by removing S_{path} and setting S_{syst} to change periodically. The circadian cycle is implemented into the intensity of the physiological photo-genic source in Eq. (13) by setting $S_{syst}(\lambda, t) = 0.9 + 0.1 \cos\left(\frac{\pi}{4}t - \frac{\pi}{2}\right)$.

morning. That diurnal variation over a range of approximately 90–110% of the mid-line level can be directly attributed to the circadian cycle. The circadian cycle is thus implemented into the intensity of the physiological photo-genic source in Eq. (A13) by setting $\mathbb{S}_{syst}(\lambda, t) = 0.9 + 0.1\cos\left(\frac{\pi}{4}t - \frac{\pi}{2}\right)$. This circadian-like systemic change results in $\mathbb{S}_{syst}(\lambda, t)$ oscillating between 1 and 0.8. The resulting photon-fluence rate as shown in Figure 6(B) varies at a cycle close to that manifested by the noisier presentation shown in panel (A).

Presentation of Spatial Asymmetry Associated with an Asymmetric Pathological Condition

The spatial asymmetry of the surface photon-fluence rate can be induced by placing a pathological photo-genic source off-center in the spherical domain. Such a possibility is demonstrated in Figure 7 in referencing the asymmetric spontaneous biophoton emission intensity that became aggregated as the tumor-load at the right axillary of a breast cancer mouse model increased (reproduced with permission from the publisher) (Zhao et al., 2017). The tumor volume is modeled as increasing exponentially (Jiang et al., 2011). The tumor volumes of respectively less than 0.5 cm in diameter, between 1 cm and 1.5 cm in diameter, and greater than 1.5 m in diameter as specified on panel (A) are modeled as $\exp\left(\frac{1}{1.5}\right)$, $\exp\left(\frac{2}{1.5}\right)$, and $\exp\left(\frac{3}{1.5}\right)$ as plotted on panel (B). The resulting numerical value of the tumor size is scaled down to 1% and used as the intensity of the pathological photo-genic source \mathbb{S}_{path} that is placed at 1 cm off-center at the right-lateral aspect and 1 cm off-center at the right anterior aspect, as illustrated in the left column of panel (C). In comparison, the centered physiological photo-genic source \mathbb{S}_{syst} is set to have an intensity of 1. The intensity ratios of the centered physiological photo-genic source \mathbb{S}_{syst} over the slightly off-centered pathological photo-genic source \mathbb{S}_{path} for the three sizes of the tumor load are thus respectively 1 vs. 0.0195, 1 vs 0.0379, and 1 vs. 0.739. The resulting photon fluence rate over the surface of the spherical tissue domain that is projected onto the middle cross-section and surrounded by a thin strip of the space beyond the tissue boundary is presented in the middle column of panel (C). The left–right asymmetry of the surface photon-fluence rate becomes

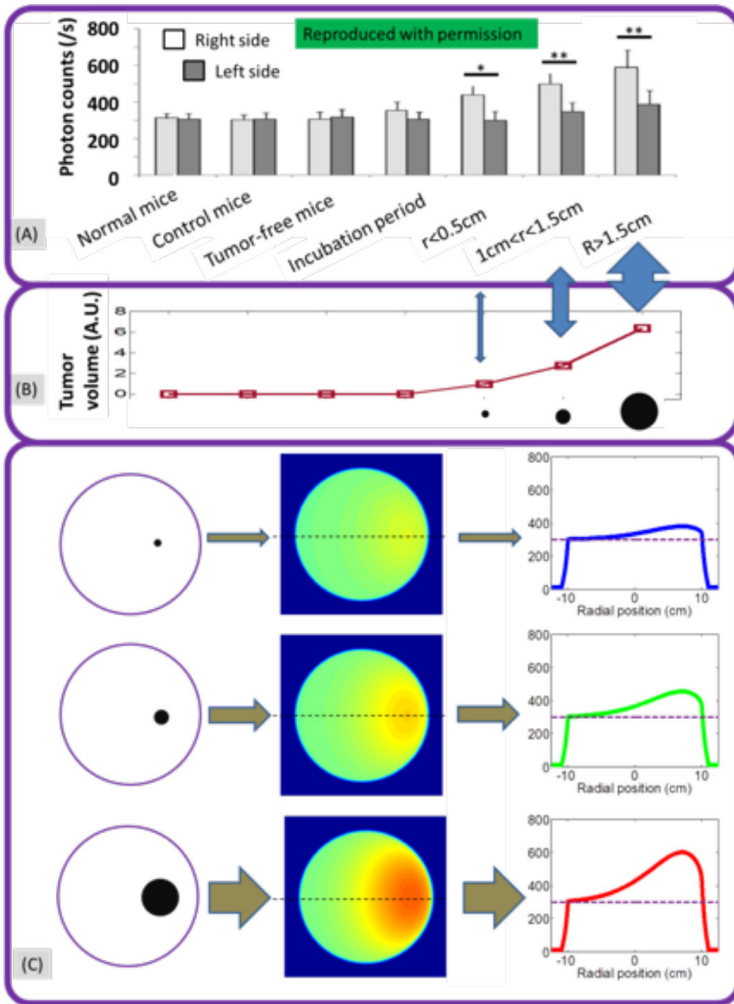


Figure 7. (A) The asymmetric biophoton emission intensity that became aggregated as the tumor-load at the right axillary of a breast cancer mouse model increased (Zhao et al., 2017). The tumor volumes of, respectively, < 0.5 cm in diameter, between 1 cm and 1.5 cm in diameter, and greater than 1.5 cm in diameter as specified on panel (A) are scaled as $\exp\left(\frac{1}{1.5}\right)$, $\exp\left(\frac{2}{1.5}\right)$, and $\exp\left(\frac{3}{1.5}\right)$ as plotted on panel (B). The resulting numerical value of the tumor size is scaled to 1% and used as the intensity of the pathological photo-genic source S_{path} that is placed at 1 cm off-center at the right-lateral aspect and 1 cm off-center at the right anterior aspect, as illustrated in the left column of panel (C). The resulting photon-fluence rate over the surface of the spherical tissue domain that is projected to the middle cross-section and surrounded by a thin strip of the space beyond the tissue boundary is presented in the middle column of panel (C). The 1-dimensional profile along the diameter crossing the 9 o'clock position to the 3 o'clock position of the 2-dimensional photon-fluence rate map of the middle column of panel (C) is given at the right column of panel (C).

pronounced as the localized pathological photo-genic source increases in intensity. The 1-dimensional profile along the diameter crossing the 9 o'clock position to the 3 o'clock position of the 2-dimensional photon-fluence rate map of the middle column of panel (C) is given at the right column. For a baseline arbitrary photon-fluence rate of 300 over the tissue domain that is least affected by the pathological photo-genic source, the global change of the maximal photon-fluence rate in the right lateral region of the side of the pathological photo-genic source increases from the baseline level to approximately 600. The pattern of the photon-fluence rate at the right lateral side is similar to that of the literature pattern of spontaneous biophoton emission shown on panel (A). Meanwhile, the maximal photon-fluence rate in the contra-lateral aspect of the pathological photo-genic source has increased slightly from the baseline, as the left-right difference becomes pronounced. This pattern of slight change of the contra-lateral normal side can also be associated with the spontaneous biophoton emission pattern shown on panel (A).

DISCUSSION

This work is intended to initiate a quantitative model-based interpretation of a few superficial patterns of steady-state spontaneous biophoton emission in humans to model human disease of holistic concern. These patterns of biophoton emission have presented associations with age, systemic physiology, and localized pathological conditions. An obvious limitation of the proposed approach is the unresolved problem regarding the exact physical mechanism of autonomic regulation of biophoton emission which, unfortunately, is prohibitive to answer and thus remains to be speculated upon at the current stage. As a result, the proposed model only simulates the general life processes from a macro perspective, by including birth, sexual maturity, aging, and possible significant pathological states of human beings as the macroscopic factors influencing the origin of biophoton emission through an oxidative stress pathway that could be influenced by autonomic neuromodulation. In addition, the contribution of organs to oxidative stress as the chemical source of photo-genesis is complex and thus discourages the simple expression of its translation

to the (single) source of biophoton emission, even though the model could serve as a starting intuitive platform that can be augmented with more complexity of the disease model in the context of photo-genesis. Another apparent limitation of this model is the arbitrary valuing of the photo-genic factor for converting the hypothetical differential change of the vivodensity to a physical source of light emission. The photo-genic factor could not be specified unless the hypothetical alternative state of the energy scaled as “vivodensity” can somehow be examined. Another limitation is the modeling of the human tissue volume as a translucent and homogeneous spherical domain, even though it perhaps be more realistic than the more commonly treated semi-infinite tissue domain. Human tissue is also extremely heterogeneous concerning photon propagation. The advantage of the present spherical tissue domain is the involvement of only one boundary, as the geometry involves essentially a radial dependency. A more practical geometry of representing human tissue volume in terms of photon propagation may be a cylindrical domain of finite-length within which the similar photon diffusion approach can be applied, and in which the heterogeneity in tissue optical properties for photon propagation can be included. Applying the photon diffusion approach to a finite-length cylindrical tissue domain would also require considering the boundary at two orientations, one along the radial dimension and the other along the polar aspect. That treatment may reveal that the strips of photon emission at the cranial and caudal aspects of the human body differ from the strips of photon emission at the lateral aspects of the human body (Van Wijk et al., 2014), a presentation that may have interesting implications for bioenergy practices. Treating heterogeneous tissue optical properties will incur considerably more complex treatment than is dealt with in this present work.

In this work, the physiological photo-genic source is hypothesized to be located at the center of the human tissue domain and concerns the systemic influence of any homeostatic causes governed by autonomic responses. Additionally, the localization of the pathological photo-genic causes at only one off-center source is rather arbitrary. But the results associated with a single off-center pathological photo-genic source can be conveniently expanded to the case of having multiple pathological conditions that each demands an individual photo-genic

source or a cluster of sources that can be weighted according to the tissue mass or volume affected. In such cases, multiple pathological photo-genic sources of different intensities (and different temporal presentations) can be localized at different positions that potentially represent their site-specific anatomy, and the spatially resolved photon-fluence rates resulting from those multiple pathological photo-genic sources can be combined in perhaps a linear format to inform the composite photon-fluence rate at the surface, and further configured in three dimensions for tomography or topography needs. For a more complicated tissue geometry and tissue with heterogeneous optical properties, the computation of the surface photon-fluence rate may be conducted by using numerical procedures such as finite-element methods (FEM) (Arridge et al., 2000) for solving photon propagation problems. Implementing numerical methods such as FEM may also allow addressing complicated pathological photo-genic causes that are better represented by the source modeled over a continuous tissue volume of arbitrary shapes or extents if they all contribute to the hypothetical photo-genesis through the oxidative stress process that ultimately involves autonomic control.

The pathological condition has been hypothetically linked in this model with neuronal control in deriving the photo-genic source term. A site of pathology that has lost autonomic control will likely lead to no change of the vivodensity, and thus a smaller or zero intensity of the photon-genic source. A smaller photo-genic source will result in a smaller superficial photon-fluence rate at the geometric side of the pathological condition, or equivalently higher superficial photon-fluence rate at the contra-lateral side. This arrangement of autonomic control has made the model output consistent with the observation of lower spontaneous biophoton emission at the hand of hemiparesis when compared with the normal contra-lateral hand (Jung et al., 2003). The validity of the photo-genic effect of autonomic control for the superficial patterns of spontaneous biophoton emission is subject to experimental examinations.

The macroscopic-scale temporal changes of the superficial photon-fluence rate have been estimated in this work for a single case of diurnal-like variation over a short 24-hour period. The approach is applicable, however, to modeling macroscopically presented, temporal

changes over a timescale much different from a day-long period. In order to evaluate the temporal changes of the superficial photon fluence rate over a longer-than-a-day scale, we will need to know how the homeostatic changes over the same timescale may alter the physiological photo-genic process. The methodological conveniences of estimating the macroscopic-scale superficial photon-fluence rate, on the other hand, may facilitate modeling the microscopic-scale temporal pattern of biophoton emission under short and strong stimulation or stress. This will require treating the photon diffusion problem as a strictly temporal problem with fast time-responses, not the steady-state problem with slower temporal modulation of the photo-genic source as is simplified in this part of the work for superficial profiling of steady-state spontaneous biophoton emission. Works based on time-domain photon propagation approaches have been demonstrated by the author to address the kinetics of the changes of biophoton emission induced by external stress that exerts significantly faster modulation to the photo-genesis (Piao, 2020a; Piao, 2020b). The theoretical outcomes of those works agree with what others have observed (Chwirot, 1988; Hagens et al., 2008) and seem to support the central hypothesis of this work.

We note that, regardless of the complexity of model approaches to explain biophoton phenomena appearing to co-exist in humans, it may become unavoidable to consider human factors in addressing the observations. And consideration of human factors will likely be plausible by implementing neuronal activities as a source of modulating biological responses that will determine the physical origin of biophoton emission, or the variation of biophoton emission as a result of external conditions. Since neuronal activities give rise to bioelectrical signals, assessing the neuro-electrical signals synchronously with the registration of any changes in biophoton emissions in humans, or a faculty of neuronal control, may provide unprecedented insights into the mechanism of biophoton emission and inter-neural communication.

CONCLUSIONS

In conclusion, we have presented an analytical hypothesis for the interpretation of a few patterns of steady-state spontaneous biophoton emission in humans, including the dependency on age,

diurnal variation, and the geometric asymmetry associated with serious asymmetrical pathological conditions. The hypothesis has assumed a collective state of autonomic neuro-energy expressed as vivodensity, which is considered to be associated with only metabolically active organisms that are also under neuronal control. This vivodensity represents the maximal coherence among the energy “modes” of neuronal control that an intelligent being represented by humans is entitled to engage in at a given time of life. This vivodensity is linked to modulating metabolic activities responsible for photo-genesis pertinent to biophoton emission. The hypothesis projects a decrease of vivodensity in humans during growth beyond puberty, with the rate of decrease dictated by a timescale set by the date of sexual maturity. The hypothesis also projects a modification of the vivodensity by the phases of systemic or homeostatic physiology. The hypothesis further postulates that the deviation of the physiology-modified vivodensity from the pre-puberty level is deteriorated by acquired organ-specific pathological conditions. A temporal differential change of vivodensity is hypothesized to ultimately cause the variations in oxidative stress that have been known to be a primary physical source of biophoton emission. The human geometry model is simplified as a homogeneous spherical domain. The resulting steady-state diffusion of the photon emitted from a photo-genic source in the human geometry model is modeled by steady-state photon diffusion incorporating an extrapolated zero-boundary condition. The physiological photo-genic source is centered, and its intensity is determined by the age and systemic physiology combined. Comparatively, an acquired asymmetric pathology sets both the intensity and the off-center position of the pathological photo-genic source. When the photo-genic sources are implemented in the photon diffusion model, the steady-state photon-fluence rate at the surface of the simplified human-representing spherical domain resembles the superficially presented patterns of age-dependency, homeostatic variation, and pathology-induced asymmetry of spontaneous biophoton emission reported in experimental studies. The analytical method has had the applicability demonstrated in a time-domain analysis, for interpreting the delayed-emission kinetics of biophoton emission under stimulation.

REFERENCES

- Arridge, S. R., Dehghani, H., Schweiger, M., & Okada, E. (2000). The finite element model for the propagation of light in scattering media: A direct method for domains with nonscattering regions. *Medical Physics*, 27(1), 252–264. <https://doi.org/10.1118/1.598868>
- Bókkon, I., Salari, V., Tuszynski, J. A., & Antal, I. (2010). Estimation of the number of biophotons involved in the visual perception of a single-object image: Biophoton intensity can be considerably higher inside cells than outside. *Journal of Photochemistry and Photobiology B: Biology*, 100(3), 160–166. <https://doi.org/10.1016/j.jphotobiol.2010.06.001>
- Bókkon, I., Vimal, R. L. P., Wang, C., Dai, J., Salari, V., Grass, F., & Antal, I. (2011). Visible light induced ocular delayed bioluminescence as a possible origin of negative afterimage. *Journal of Photochemistry and Photobiology B: Biology*, 103(2), 192–199. <https://doi.org/10.1016/j.jphotobiol.2011.03.011>
- Boveris, A., Cadenas, E., Reiter, R., Filipkowski, M., Nakase, Y., & Chance, B. (1980). Organ chemiluminescence: Noninvasive assay for oxidative radical reactions. *Proceedings of the National Academy of Sciences USA*, 77(1), 347–351. <https://doi.org/10.1073/pnas.77.1.347>
- Boveris, A., Puntarulo, S. A., Roy, A. H., & Sanchez, R. A. (1984). Spontaneous chemiluminescence of soybean embryonic axes during imbibition. *Plant Physiology*, 76(2), 447–451. <https://doi.org/10.1104/pp.76.2.447>
- Burgos, R. C., Cervinková, K., van der Laan, T., Ramautar, R., van Wijk, E. P. A., Cifra, M., Koval, S., Berger, R., Hankemeier, T., & van der Greef, J. (2016). Tracking biochemical changes correlated with ultra-weak photon emission using metabolomics. *Journal of Photochemistry and Photobiology B: Biology*, 163, 237–245. <https://doi.org/10.1016/j.jphotobiol.2016.08.030>
- Cadenas, E. (1984). Biological chemiluminescence. *Photochemistry and Photobiology*, 40(6), 823–830. <https://doi.org/10.1111/j.1751-1097.1984.tb04657.x>
- Cadenas, E., Boveris, A., & Chance, B. (1980). Low-level chemiluminescence of bovine heart submitochondrial particles. *Biochemical Journal*, 186(3), 659–667. <https://doi.org/10.1042/bj1860659>
- Caswell, J. M., Dotta, B. T., & Persinger, M. A. (2014). Cerebral biophoton emission as a potential factor in non-local human-machine interaction. *NeuroQuantology*, 12(1), 1–11. <https://doi.org/10.14704/NQ.2014.12.1.713>
- Chwirot, W. B. (1988). Ultraweak photon emission and anther meiotic cycle in *Larix europaea* (experimental investigation of Nagl and Popp's electromagnetic model of differentiation). *Experientia*, 44(7), 594–599. <https://doi.org/10.1007/BF01953307>
- Cifra, M., & Pospišil, P. (2014). Ultra-weak photon emission from biological samples: Definition, mechanisms, properties, detection and applications. *Journal of Photochemistry and Photobiology B: Biology*, 139, 2–10. Cifra, M., van Wijk, E., Koch, H., Bosman, S., & Van Wijk, R. (2007). Spontaneous ultra-weak photon emission from human hands is time dependent. *Radioengineering*, 16(2), 15–19. <https://doi.org/10.1016/j.jphotobiol.2014.02.009>

- Cohen, S., & Popp, F. A. (1997). Biophoton emission of the human body. *Journal of Photochemistry and Photobiology, Biology B: Biology*, 40(2), 187–189. [https://doi.org/10.1016/S1011-1344\(97\)00050-X](https://doi.org/10.1016/S1011-1344(97)00050-X)
- Cohen, S., & Popp, F. A. (2003). Biophoton emission of human body. *Indian Journal of Experimental Biology*, 41(5), 440–445.
- Contini, D., Martelli, F., & Zaccanti, G. (1997). Photon migration through a turbid slab described by a model based on diffusion approximation. I. Theory. *Applied Optics*, 36(19), 4587–4599. <https://woi.org/10.1364/ao.36.004587>
- Devaraj, B., Usa, M., & Inaba, H. (1997). Biophotons: Ultraweak light emission from living systems. *Current Opinion in Solid State & Materials Science* 2(2), 188–193. [https://doi.org/10.1016/S1359-0286\(97\)80064-2](https://doi.org/10.1016/S1359-0286(97)80064-2)
- Fedorova, G. F., Trofimov, A. V., Vasil'ev, R. F., & Veprintsev, T. L. (2007). Peroxy-radical-mediated chemiluminescence: Mechanistic diversity and fundamentals for antioxidant assay. *Arkhivoc*, 8, 163–215. <https://doi.org/10.3998/ark.5550190.0008.815>
- Gallas, J. M., & Eisner, M. (1987). Fluorescence of melanin—dependence upon excitation wavelength and concentration. *Photochemistry and Photobiology*, 45(5), 595–600. <https://doi.org/10.1111/j.1751-1097.1987.tb07385.x>
- Hagens, R., Khabiri, F., Schreiner, V., Wenck, H., Wittern, K.-P., Duchstein, H.-J., & Mei, W. (2008). Non-invasive monitoring of oxidative skin stress by ultraweak photon emission measurement. II: Biological validation on ultraviolet A-stressed skin. *Skin Research and Technology*, 14(1), 112–120. <https://doi.org/10.1111/j.1600-0846.2007.00207.x>
- Haraguchi, S., Kotake, J., Chen, W., Parkhomtchouk, D. V., Zhang, T., & Yamamoto, M. (2001). Biophoton change by mental concentration. *Journal of International Society of Life Information Science*, 19(2), 373–380.
- Haskell, R. C., Svaasand, L. O., Tsay, T. T., Feng, T. C., McAdams, M. S., & Tromberg, B. J. (1994). Boundary conditions for the diffusion equation in radiative transfer. *Journal of the Optical Society of America, A: Optics, Image Science, and Vision*, 11(10), 2727–2741. <https://doi.org/10.1364/josaa.11.002727>
- Havaux, M., Triantaphylidès, C., & Genty, B. (2006). Autoluminescence imaging: A non-invasive tool for mapping oxidative stress. *Trends in Plant Science*, 11(10), 480–484.
- He, M., Sun, M., van Wijk, E., van Wietmarschen, H., van Wijk, R., Wang, Z., Wang, M., Hankemeier, T., & van der Greef, J. (2016). A Chinese literature overview on ultra-weak photon emission as promising technology for studying system-based diagnostics. *Complementary Therapies in Medicine*, 25, 20–26. <https://doi.org/10.1016/j.ctim.2015.12.015>
- Ishimaru, A. (1989). Diffusion of light in turbid material. *Applied Optics*, 28(12), 2210–2215. <https://doi.org/10.1364/AO.28.002210>
- Ives, J. A., van Wijk, E. P. A., Bat, N., Crawford, C., Walter, A., Jonas, W. B., van Wijk, R., & van der Greef, J. (2014). Ultraweak photon emission as a non-invasive health assessment: A systematic review. *PLoS One* 9(2), e87401. <https://doi.org/10.1371/journal.pone.0087401>
- Jiang, Z., Piao, D., Bartels, K. E., Holyoak, G. R., Ritchey, J. W., Ownby, C. L., Rock, K., & Slobodov, G. (2011). Transrectal ultrasound-integrated spectral optical tomography of hypoxic progression of a regressing tumor in a canine

- prostate. *Technology in Cancer Research & Treatment*, 10(6), 519–531. <https://doi.org/10.1177/153303461101000603>
- Joines, W. T., Baumann, S. B., & Kruth, J. G. (2012). Electromagnetic emission from humans during focused intent. *Journal of Parapsychology*, 76(2), 275–294.
- Jung, H.-H., Woo, W.-M., Yang, J.-M., Choi, C., Lee, J., Yoon, G., Yang, J.-S., Lee, S., & Soh, K.-S. (2003). Left-right asymmetry of biophoton emission from hemiparesis patients. *Indian Journal of Experimental Biology*, 41(5), 452–456.
- Jung, H.-H., Yang, J.-M., Woo, W.-M., Choi, C., Yang, J.-S., & Soh, K.-S. (2005). Year-long biophoton measurements: Normalized frequency count analysis and seasonal dependency. *Journal of Photochemistry and Photobiology B: Biology*, 78(2), 149–154. <https://doi.org/10.1016/j.jphotobiol.2004.08.002>
- Kalaji, H. M., Goltsev, V., Bosa, K., Allakhverdiev, S. I., Strasser, R. J., & Govindjee (2012). Experimental in vivo measurements of light emission in plants: A perspective dedicated to David Walker. *Photosynthesis Research*, 114(2), 69–96.
- Kayatz, P., Thumann, G., Luther, T. T., Jordan, J. F., Bartz-Schmidt, K. U., Esser, P. J., & Schraermeyer, U. (2001). Oxidation causes melanin fluorescence. *Investigative Ophthalmology & Visual Science*, 42(1), 241–246.
- Kobayashi, M., Iwasa, T., & Tada, M. (2016). Polychromatic spectral pattern analysis of ultra-weak photon emissions from a human body. *Journal of Photochemistry and Photobiology B: Biology*, 159, 186–190. <https://doi.org/10.1016/j.jphotobiol.2016.03.037>
- Kobayashi, M., Kikuchi, D., & Okamura, H. (2009). Imaging of ultraweak spontaneous photon emission from human body displaying diurnal rhythm. *PLoS One*, 4(7), e6256. <https://doi.org/10.1371/journal.pone.0006256>
- Kobayashi, K., Okabe, H., Kawano, S., Hidaka, Y., & Hara, K. (2014). Biophoton emission induced by heat shock. *PLoS One*, 9(8), e105700. <https://doi.org/10.1371/journal.pone.0105700>
- Moraes, T. A., Barlow, P. W., Klingelé E., & Gallep, C. M. (2012). Spontaneous ultra-weak light emissions from wheat seedlings are rhythmic and synchronized with the time profile of the local gravimetric tide. *Naturwissenschaften*, 99(6), 465–472. <https://doi.org/10.1007/s00114-012-0921-5>
- Musumeci, F., Scordino, A., & Triglia, A. (1997). Delayed luminescence from simple biological systems. *Rivista di Biologia*, 90(1), 95–110.
- Nakamura, H., Kokubo, H., Parkhomtchouk, D. V., Chen, W., Tanaka, M., Zhang, T., Kokado, T., Yamamoto, M., & Fukuda, N. (2000). Biophoton and temperature changes of human hand during Qigong. *Journal of International Society of Life Information Science*, 18(2), 418–422.
- Pederzoli, L., Giroladini, W., Prati, E., & Tressoldi, P. (2017). The physics of mind-matter interaction at a distance. *NeuroQuantology*, 15(3), 114–119. <https://doi.org/10.2139/ssrn.2968430>
- Persinger, M. A., & St-Pierre, L. S. (2011). The biophysics at death: Three hypotheses with potential application to paranormal phenomena. *NeuroQuantology*, 9(1), 36–40. <https://doi.org/10.14704/nq.2011.9.1.388>
- Piao, D. (2020a). On the stress-induced photon emission from organism: I, will the scattering-limited delay affect the temporal course? *SN Applied Sciences*, 2, 1566.

- <https://doi.org/10.1007/s42452-020-03346-1>
- Piao, D. (2020b). On the stress-induced photon emission from organism: II, how will the stress-transfer kinetics affect the photo-genesis? *SN Applied Sciences*, 2, 1556. <https://doi.org/10.1007/s42452-020-03347-0>
- Piao, D., Barbour, R. L., Graber, H. L., & Lee, D. C. (2015). On the geometry dependence of differential pathlength factor for near-infrared spectroscopy. I. Steady-state with homogeneous medium. *Journal of Biomedical Optics*, 20(10), 105005. <https://doi.org/10.1117/1.JBO.20.10.105005>
- Quickenden, T. I., & Que Hee, S. S. (1974). Weak luminescence from the yeast *Saccharomyces cerevisiae* and the existence of mitogenetic radiation. *Biochemical and Biophysical Research Communications*, 60(2), 764–770. [https://doi.org/10.1016/0006-291X\(74\)90306-4](https://doi.org/10.1016/0006-291X(74)90306-4)
- Rahnama, M., Tuszyński, J. A., Bókkon, I., Cifra, M., Sardar, P., & Salari, V. (2011). Emission of mitochondrial biophotons and their effect on electrical activity of membrane via microtubules. *Journal of Integrative Neuroscience*, 10(1), 65–88. <https://doi.org/10.1142/S0219635211002622>
- Reddy, J. S. K. (2016). Could ‘biophoton emission’ be the reason for mechanical malfunctioning at the moment of death? *NeuroQuantology*, 14(4), 806–809.
- Rice, M. E., Forman, R. E., Chen, B. T., Avshalumov, M. V., Cragg, S. J., & Drew, K. L. (2002). Brain antioxidant regulation in mammals and anoxia-tolerant reptiles: Balanced for neuroprotection and neuromodulation. *Comparative Biochemistry and Physiology, Part C: Toxicology and Pharmacology*, 133(4), 515–525.
- Rubik, B., & Jabs, H. (2017). Effects of intention, energy healing, and mind-body states on biophoton emission. *Cosmos and History: The Journal of Natural and Social Philosophy*, 13(2), 227–247.
- Salari, V., Scholkmann, F., Vimal, R. L. P., Császár, N., Aslani, M., & Bókkon, I. (2017). Phosphenes, retinal discrete dark noise, negative afterimages and retinogeniculate projections: A new explanatory framework based on endogenous ocular luminescence. *Progress in Retinal and Eye Research*, 60, 101–119.
- Sarna, S., Sahi, T., Koskenvuo, M., & Kaprio, J. (1993). Increased life expectancy of world class male athletes. *Medicine & Science in Sports & Exercise*, 25(2), 237–244.
- Sauermann, G., Mei, W. P., Hoppe, U., & Stäb, F. (1999). Ultraweak photon emission of human skin in vivo: Influence of topically applied antioxidants on human skin. *Methods in Enzymology*, 300, 419–428. [https://doi.org/10.1016/S0076-6879\(99\)00147-0](https://doi.org/10.1016/S0076-6879(99)00147-0)
- Slawinski, J., Ezzahir, A., Godlewski, M., Kwiecinska, T., Rajfur, Z., Sitko, D., & Wierzuchowska, D. (1992). Stress-induced photon emission from perturbed organisms. *Experientia*, 48(11–12), 1041–1058. <https://doi.org/10.1007/BF01947992>
- Sun, M., Van Wijk, E., Koval, S., Van Wijk, R., He, M., Wang, M., Hankemeier, T., & van der Greef, J. (2017). Measuring ultra-weak photon emission as a non-invasive diagnostic tool for detecting early-stage type 2 diabetes: A step toward personalized medicine. *Journal of Photochemistry and Photobiology B: Biology*, 166, 86–93. <https://doi.org/10.1016/j.jphotobiol.2016.11.013>
- Tsuchida, K., Iwasa, T., & Kobayashi, M. (2019). Imaging of ultraweak photon

- emission for evaluating the oxidative stress of human skin. *Journal of Photochemistry and Photobiology B: Biology*, 198, 111562. <https://doi.org/10.1016/j.jphotobiol.2019.111562>
- Van Wijk, R., Van Wijk, E. P. A., van Wietmarschen, H. A., & van der Greef, J. (2014). Towards whole-body ultra-weak photon counting and imaging with a focus on human beings: A review. *Journal of Photochemistry and Photobiology B: Biology*, 139, 39–46. <https://doi.org/10.1016/j.jphotobiol.2013.11.014>
- Wang, J., & Yu, Y. (2009). Relationship between ultra-weak bioluminescence and vigour or irradiation dose of irradiated wheat. *Luminescence*, 24(4), 209–212. <https://doi.org/10.1002/bio.1096>
- Wang, C., Bókkon, I., Dai, J., & Antal, I. (2011). Spontaneous and visible light-induced ultraweak photon emission from rat eyes. *Brain Research*, 1369, 1–9. <https://doi.org/10.1016/j.brainres.2010.10.077>
- Wang, Z., Wang, N., Li, Z., Xiao, F., & Dai, J. (2016). Human high intelligence is involved in spectral redshift of biophotonic activities in the brain. *Proceedings of the National Academy of Sciences USA*, 113(31), 8753–8758. <https://doi.org/10.1073/pnas.1604855113>
- Wilson, H. R., & Cowan, J. D. (1972). Excitatory and inhibitory interactions in localized populations of model neurons. *Biophysics Journal*, 12(1), 1–24. [https://doi.org/10.1016/S0006-3495\(72\)86068-5](https://doi.org/10.1016/S0006-3495(72)86068-5)
- Yang, W., Zhou, W., Lv, Y., & Song, W. (1995). Ultraweak photon emission experimental study on the torso meridian of 80 healthy people. *Shenzhen Zhongxiyi Jiehe Zazhi*, 5(3), 1–3.
- Yang, W. Y., Zhou, W. X., Song, W., & Lv, Y. (1996). Ultraweak photon emission experimental study on the four limbs meridian of 130 healthy people. *Shanghai Zhenjiu Zazhi*, 15(1), 34–35.
- Zhang, A., Piao, D., Bunting, C. F., & Pogue, B. W. (2010). Photon diffusion in a homogeneous medium bounded externally or internally by an infinitely long circular cylindrical applicator. I. Steady-state theory. *Journal of the Optical Society of America, A: Optics, Image Science, and Vision*, 27(3), 648–662. <https://doi.org/10.1364/JOSAA.27.000648>
- Zhang, J., Yu, W., Sun, T., & Popp, F.-A. (1997). Spontaneous and light-induced photon emission from intact brains of chick embryos. *Science in China Series C: Life Sciences*, 40(1), 43–51.
- Zhao, X., Pang, J., Fu, J., Wang, Y., Yang, M., Liu, Y., Fan, H., Zhang, L., & Han, J. (2017). Spontaneous photon emission: A promising non-invasive diagnostic tool for breast cancer. *Journal of Photochemistry and Photobiology B*, 166, 232–238. <https://doi.org/10.1016/j.jphotobiol.2016.12.009>
- Zhao, X., van Wijk, E., Yan, Y., van Wijk, R., Yang, H., Zhang, Y., & Wang, J. (2016). Ultra-weak photon emission of hands in aging prediction. *Journal of Photochemistry and Photobiology B: Biology*, 162, 529–534. <https://doi.org/10.1016/j.jphotobiol.2016.07.030>
- Zheng, R., Lu, J., Lin, Y., & Zhang, M. (1983). The studies of the relationship between human body surface ultraweak luminescence and certain physiological state. *Shanghai Zhongyiyao Zazhi*, 1(1), 44–47.

APPENDIX

Steady-State Photon Diffusion in an Unbounded Medium of Spherical Geometry

With the placement of a steady-state photo-genic source in the spherical tissue domain representing the human body, the steady-state propagation of the photon in the spherical domain that is several orders greater than the photon-scattering path-length in a biological tissue can be readily modeled by the diffusion approximation to the radiative transfer equation (Ishimaru, 1989). The human body is treated in the present work as a globally homogeneous diffusive medium containing localized steady-state spatially impulsive photo-genic sources. The diffusive tissue medium is characterized by the following properties: absorption coefficient μ_a [unit: cm^{-1}], reduced scattering coefficient μ'_s [unit: cm^{-1}], diffusion coefficient $D = 1/[3(\mu_a + \mu'_s)]$ [unit: cm], and effective attenuation coefficient $\mu_{eff} = \sqrt{\mu_a/D}$ [unit: cm^{-1}]. For a field or detection position at $\vec{\chi} = (\mathbf{r}, \theta, \varphi)$ within the globally homogeneous tissue domain including that on the tissue-air boundary, the steady-state photon-fluence rate $\Psi(\vec{\chi})$ (unit: $\text{Ws}^{-1}\text{cm}^{-2}$) satisfies the following governing equation (Contini et al., 1997):

$$\nabla^2 \Psi(\vec{\chi}) - \frac{\mu_a}{D} \Psi(\vec{\chi}) = -\frac{S(\vec{\chi})}{D} \quad (\text{A1})$$

where $S(\vec{\chi})$ is a source term, which is also subject to a boundary condition as all boundary-involved electromagnetic problems are. For an infinite homogeneous medium containing a steady-state point source at $\vec{\chi}'$ with an intensity S as represented by $S \cdot \delta(\vec{\chi}')$, Eq. (A1) has the well-known Green's function solution of (Zhang et al., 2010):

$$\Psi(\vec{\chi}, \vec{\chi}') = \frac{S}{4\pi D} \frac{1}{|\vec{\chi} - \vec{\chi}'|} \exp(-\mu_{eff} |\vec{\chi} - \vec{\chi}'|) \quad (\text{A2})$$

Eq. (A2) can also be written in the following form of Eigen function expansion (Piao et al., 2015):

$$\Psi(\vec{\chi}, \vec{\chi}') = \frac{S}{D} (\mu_{eff}) \sum_{l=0}^{\infty} [i_l(\mu_{eff} r_{<}) \cdot k_l(\mu_{eff} r_{>})] \sum_{m=-l}^l [Y_{lm}^*(\theta', \phi') \cdot Y_{lm}(\theta, \phi)] \quad (\text{A3})$$

where i_l and k_l are respectively the l -th order modified spherical Bessel function of the first and the second kinds, $r_{<}$ and $r_{>}$ are, respectively, the smaller and greater radial coordinates between the source and the detector, and Y_{lm} is the spherical harmonics function.

Treatment of the Boundary Condition Associated with Steady-State Biophoton Emission from a Spherical Surface

With regard to the effect on photon-fluence rate by the tissue–air boundary, it has been established that the photon-fluence rate does not become zero at a field position immediately beyond the tissue boundary; instead, a more accurate treatment of an extrapolated zero-boundary condition sets zero for the photon-fluence rate at a distance away from the tissue boundary—the so-called extrapolated zero-boundary (Haskell et al., 1994). Figure 3 with the implementation of the extrapolated zero-boundary is illustrated in Figure A1. A field \vec{x} point on or beyond the spherical tissue boundary locates at (r, θ, ϕ) with $r \geq R_0 + R_b$. The application of the extrapolated zero-

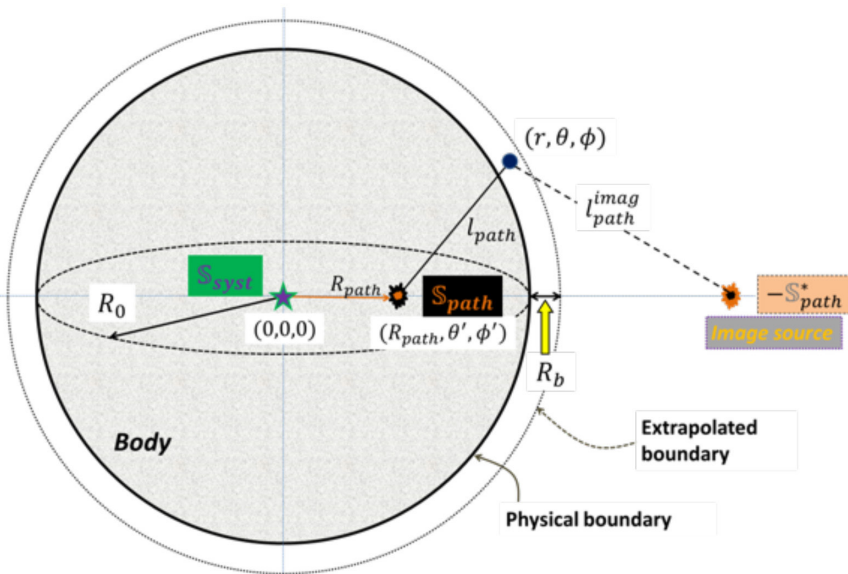


Figure A1. The human body containing a physiological photo-genetic source of S_{sys} at the center of the spherical domain, and a single pathological photo-genetic S_{path} source at $(R_{path}, 0, 0)$. The photon emitted by a photo-genetic source diffuses in the human body and encounters a refractive index discontinuity at the body boundary. The effect of the tissue–air boundary is accounted for by setting the photon-fluence rate at an imaginary boundary extrapolated from the physical boundary at a distance of R_b . The image of the single pathological photo-genetic source S_{path} is located at the radial direction S_{path} of due to the obvious symmetry. The intensity of the image of the single pathological photo-genetic source S_{path} may become $-S_{path}$ in the case of the tissue becoming a semi-infinite domain.

boundary condition to the photon fluence associated with any source within the tissue medium is satisfied by introducing an “image” of the source with respect to the extrapolated zero-boundary that is co-centric with and at a radial distance of $R_b = 2AD$ outward from the physical boundary (Piao et al., 2015) where

$$A = (1 + \xi)/(1 - \xi), \xi = -1.440n^{-2} + 0.710n^{-1} + 0.668 + 0.0636n,$$

and n is the refractive index of the air-bounding tissue. As the composite photon-fluence rate resulting from both the physical source in the tissue medium and the image of it becomes zero at the extrapolated zero-boundary, the composite positive photon-fluence rate elsewhere resulting from the same two sources of one being physical and the other being imaginary thus become the solution in the associated physical space within the body volume or beyond the boundary, according to the unique characteristics of all the electromagnetic properties.

For the pathological photo-genic source S_{path} located off-center at $(R_{path}, \theta', \phi')$, the geometric symmetry determines that the image of it with respect to the extrapolated zero-boundary must be located along the same radial direction. The source S_{path} and its image with respect to the extrapolated zero-boundary thus collectively set at zero the photon-fluence rate on the extrapolated zero-boundary. Based on Eq. (A3), the photon-fluence rate associated with the pathological photo-genic source S_{path} and evaluating on the extrapolated zero-boundary, for which the source locates at $r_< = R_{path}$ and the field point locates at $r_> = R_0 + R_b$, is

$$\Psi_{path}|_{extra} = S_{path} \frac{1}{D} (\mu_{eff}) \sum_{l=0}^{\infty} i_l [\mu_{eff} \cdot (R_{path})] \cdot k_l [\mu_{eff} (R_0 + R_b)] \sum_{m=-l}^l Y_{lm}^*(\theta', \phi') Y_{lm}(\theta, \phi) \tag{A4}$$

where the notation “ $left|right$ ” indicates evaluating the “left” term as the source and the “right” term as the field position. Note that any “ l ”th order (or moment) of the pathological photo-genic source has the same intensity as S_{path} . Similarly, the photon-fluence rate associated with the image of the pathological photo-genic source, and evaluated on the extrapolated zero-boundary, for which the source now is located at a radial position of a to-be-determined $r_>$ and the detector located at $r_< = R_0 + R_b$, is

$$\Psi_{path}^{imag}|_{extra} = \frac{1}{D} (\mu_{eff}) \sum_{l=0}^{\infty} S_l^* \cdot i_l [\mu_{eff} (R_0 + R_b)] \cdot k_l [\mu_{eff} r_>] \sum_{m=-l}^l Y_{lm}^*(\theta', \phi') Y_{lm}(\theta, \phi) \tag{A5}$$

where the term S_l^* is different for different “ l ” (or moment). Based on the essence of “image-source” (Zhang et al., 2010; Piao et al., 2015), the two unknown terms S_l^* and $r_>$ associated with the l -th order (or moment) “image” source (the component) can be expressed by a single unknown term S_l associated with the same order (or moment) of the actual pathological photo-genic source S_{path} located within the tissue at $(R_{path}, \theta', \phi')$, (the i_l component), as the following:

$$S_l^* \cdot k_l[\mu_{eff}r_>] = S_l \cdot i_l[\mu_{eff}(R_{path})] \tag{A6}$$

Applying the extrapolated zero-boundary condition of

$$\Psi_{path}|_{extra} + \Psi_{path}^{imag}|_{extra} = 0$$

leads to

$$S_l = -S_{path} \frac{k_l[\mu_{eff}(R_0+R_b)]}{i_l[\mu_{eff}(R_0+R_b)]} \quad l = 0,1,2, \dots \tag{A7}$$

Now for the photon-fluence rate associated with the pathological photo-genic source at $(R_{path}, \theta', \phi')$, but evaluating at a field point between the body boundary and the extrapolated zero-boundary, the source still locates at $r_< = R_{path}$ but the detector or the field point locates at $r_> = R_0 + \Delta r$, where $\Delta r \in [0, R_b]$. For the photon-fluence rate associated with the image of the pathological photo-genic source and also evaluating at a field point between the body boundary and the extrapolated zero-boundary, the field point now is located at $r_< = R_0 + \Delta r$ and the source terms are known through Eqs. (A6) and (A7). Collectively the composite photon-fluence rate originating from a pathological photo-genic source at $(R_{path}, \theta', \phi')$, and sensed by a detector or field point at $(R_0 + \Delta r, \theta, \phi)$ between the body boundary and the extrapolated zero-boundary becomes:

$$\begin{aligned} \Psi_{path} &= \Psi_{path}|_{field} + \Psi_{path}^{imag}|_{field} \\ &= \frac{S_{path}}{D} (\mu_{eff}) \sum_{l=0}^{\infty} i_l[\mu_{eff}(R_{path})] \cdot k_l[\mu_{eff}(R_0 + \Delta r)] \sum_{m=-l}^l Y_{lm}^*(\theta', \phi') Y_{lm}(\theta, \phi) \\ &- \frac{S_{path}}{D} (\mu_{eff}) \sum_{l=0}^{\infty} i_l[\mu_{eff}(R_0 + \Delta r)] i_l[\mu_{eff}(R_{path})] \cdot \frac{k_l[\mu_{eff}(R_0 + R_b)]}{i_l[\mu_{eff}(R_0 + R_b)]} \sum_{m=-l}^l Y_{lm}^*(\theta', \phi') Y_{lm}(\theta, \phi) \\ &= \frac{S_{path}}{D} (\mu_{eff}) \sum_{l=0}^{\infty} i_l[\mu_{eff}(R_{path})] \cdot k_l[\mu_{eff}(R_0 + \Delta r)] \sum_{m=-l}^l Y_{lm}^*(\theta', \phi') Y_{lm}(\theta, \phi) \\ &\quad \left\{ 1 - \frac{i_l[\mu_{eff}(R_0+\Delta r)] k_l[\mu_{eff}(R_0+R_b)]}{k_l[\mu_{eff}(R_0+\Delta r)] i_l[\mu_{eff}(R_0+R_b)]} \right\} \end{aligned} \tag{A8}$$

Equation (A8) contains two parts: the “1” in the bracket represents the infinite-medium contribution to the photon-fluence rate by the pathological photo-genic source S_{path} that can be expressed in the simple form of Eq. (A2); and the other term in the bracket scales the infinite-medium contribution to the photon-fluence rate by the image of the pathological photo-genic S_{path} source with respect to the former one. By using some analytics of the modified spherical Bessel function and Eq. (A2), Eq. (A8) is converted to the following form (Piao et al., 2015)

$$\Psi_{path} = \frac{S_{path}}{4\pi D} \frac{1}{l_{path}} \exp(-\mu_{eff} l_{path}) \left\{ 1 - \frac{I_{l+1/2}[\mu_{eff}(R_0+\Delta r)] K_{l+1/2}[\mu_{eff}(R_0+R_b)]}{K_{l+1/2}[\mu_{eff}(R_0+\Delta r)] I_{l+1/2}[\mu_{eff}(R_0+R_b)]} \right\} \tag{A9}$$

where $I_{l+\frac{1}{2}}$ and $K_{l+\frac{1}{2}}$ are respectively the $(l + \frac{1}{2})$ -th order modified Bessel function of the first and the second kinds. For a human body simplified as a spherical domain, it is easy to have an R_0 (i.e., 10 cm) that is substantially greater than 10 times $1/\mu_{eff}$ and to have the $\frac{R_0}{1/\mu_{eff}}$ term in the bracket of Eq. (A9) approximated by

$$\frac{I_{l+1/2}[\mu_{eff}(R_0 + \Delta r)] K_{l+1/2}[\mu_{eff}(R_0 + R_b)]}{K_{l+1/2}[\mu_{eff}(R_0 + \Delta r)] I_{l+1/2}[\mu_{eff}(R_0 + R_b)]} = \exp[-2\mu_{eff}(R_b - \Delta r)] \tag{A10}$$

Thus, Eq. (A9) will be changed to a trivial form of

$$\Psi_{path} = \frac{S_{path}}{4\pi D} \frac{1}{l_{path}} \exp(-\mu_{eff} l_{path}) \{ 1 - \exp[-2\mu_{eff}(R_b - \Delta r)] \} \tag{A11}$$

Eq. (A11), which is associated with the pathological photo-genic source of S_{path} , conveniently satisfies the condition of producing a zero composite photon-fluence rate at the extrapolated zero-boundary, whereupon Eq. (A11) also determines that the photon-fluence rate associated $\Delta r = R_b$. with the pathological photo-genic source of which decreases monotonically from the body S_{path} boundary to the extrapolated zero-boundary. One can find that a hypothetical movement of the photo-genic source like the pathological one from toward the center of the S_{path} spherical domain (R_{path}, θ, ϕ) , can maintain the boundary-resulted composite photon-fluence rate in the form of Eq. (A11), with the length dimension l_{path} varying according to the position of the photo-genic source. The hypothetical experiment infers that

the boundary-resulted composite photon-fluence rate at a field point at $(R_0 + \Delta r, \theta, \varphi)$ in association with a physiological photo-genic source \mathbb{S}_{syst} located at the center of the spherical domain can be represented as the following:

$$\Psi_{syst} = \frac{\mathbb{S}_{syst}}{4\pi D} \frac{1}{l_{syst}} \exp(-\mu_{eff} l_{syst}) \{1 - \exp[-2\mu_{eff}(R_b - \Delta r)]\} \quad (A12)$$

where l_{syst} is the distance from the physiological photo-genic source to the field point. When both the physiological photo-genic source \mathbb{S}_{syst} and the pathological photo-genic source \mathbb{S}_{path} are considered as the origins of the photon emission causing photon distribution beyond the spherical boundary, the composite photon-fluence rate at a field point $(R_0 + \Delta r, \theta, \varphi)$ is thus the combination of the respective photon-fluence rates of Eqs. (A1) and (A12), as the following:

$$\Psi_{total} = \frac{1}{4\pi D} \left[\mathbb{S}_{syst} \frac{1}{l_{syst}} \exp(-\mu_{eff} l_{syst}) + \mathbb{S}_{path} \frac{1}{l_{path}} \exp(-\mu_{eff} l_{path}) \right] \{1 - \exp[-2\mu_{eff}(R_b - \Delta r)]\}$$

(A13)

Regarding Slow Photon Sourcing for Steady-State Biophoton Emission

Ideally, the temporal profile of the photons measured at the tissue surface shall be the convolution of the source temporal profile with the temporal point-spread function of the photon diffusion process. All changes of biophotons measured at the surface over the scales assessed in this work can be safely treated as infinitely large compared with the time that a biophoton takes to propagate from a site of photo-genesis to the surface. This essentially makes the surface measurement of biophotons follow exactly the temporal pace of the photo-genesis term, which shall reflect what has happened due to physiological, environmental, or pathological conditions.